Ceramics International 46 (2020) 9086–9095

Contents lists available at ScienceDirect

Ceramics International

journal homepage: www.elsevier.com/locate/ceramint

Manufacturing and characterization of mechanical, biological and dielectric properties of hydroxyapatite-barium titanate nanocomposite scaffolds

Mina Tavangar[a], Fatemeh Heidari[a,*], Raziye Hayati[a], Fahimeh Tabatabaei[b,c], Daryoosh Vashaee[d], Lobat Tayebi[c]

[a] Department of Materials Engineering, Yasouj University, Yasouj, 75918-74934, Iran
[b] Department of Dental Biomaterials, School of Dentistry, Shahid Beheshti University of Medical Sciences, Tehran, Iran
[c] Marquette University School of Dentistry, Milwaukee, WI, USA
[d] Department of Electrical and Computer Engineering, NC State University, Raleigh, NC, 27695, United States

ARTICLE INFO

Keywords:
Nanocomposite
Barium titanate
Mechanical property
Piezoelectric property
Biocompatibility

ABSTRACT

In this research, hydroxyapatite (HA)-based ceramics were produced as suitable ceramic implants for orthopedic applications. To improve the physical, mechanical, electrical and biological properties of pure HA, we developed composite scaffolds of HA-barium titanate (BT) by cold isostatic pressing and sintering. Microstructure, crystal phases, and molecular structure were analyzed by using scanning electron microscopy (SEM), transmission electron microscopy (TEM), X-ray diffraction (XRD) and Fourier transform infrared spectroscopy (FTIR), respectively. Bulk density values were measured using the Archimedes method. The effect of different percentages of BT on cell proliferation, viability, and ALP activity of dental pulp stem cells (DPSCs) was assessed by ProstoBlue assay, Live/Dead staining, and p-NPP assay. The obtained results indicate that the HA-BT scaffolds possess higher compressive strength, toughness, density, and hardness compared with pure HA scaffolds. After immersing the scaffold in SBF solution, more deposited apatite appeared on the HA-BT, which results in rougher surface on this scaffold thanpure HA. Electrical properties of HA in the presence of BT are improved. Based on the results of cell culture experiments, composites containing 40, 50 and 60 %wt of BT have excellent biocompatibility, with the best results occurring for the sample with 50 %wt BT.

1. Introduction

Today, the growing demand for bone-based artificial materials has led to the development of research into design, manufacture, and characterization of nanostructured porous biomaterials for remodeling and repairing the damaged bone tissues [1,2]. Since natural bone is a porous nanocomposite material with electrical activity, many efforts have been made to find alternative materials with the same electrical properties as normal bone. The piezoelectric properties of bone were first shown by Fukada and Yasuda [3], in which positive and negative permanent electrical charges were created due to mechanical stress caused by daily activities following some structural changes in the bone. It should be noted that the direct and indirect piezoelectric properties of the bone and the formation of positive and negative charges contribute to the activity of bone-resorbing (osteoclasts) and bone-forming (osteoblast) cells, respectively [4–6].

In tissue engineering, different shapes and types of metallic, ceramic, polymeric, and even composite implants are used. Among the above mentioned scaffolds, ceramic types are the most widely used ones, due to their mechanical strength, corrosion resistance, and, consequently, very high and suitable bioactivity compared to other materials [5]. During the last forty years, a calcium phosphate-based ceramic—synthetic hydroxyapatite (HA)—with the chemical formula of $Ca_{10}(Po_4)_6(OH)_2$ and hexagonal structure [7], and high chemical and structural similarity to the natural bone and tooth has been widely used in biomaterials [8]. Among the wide range of calcium phosphates, the exact ratio between calcium and phosphorus (Ca/P) is a significant factor affecting its solubility. The low calcium to phosphorus ratio (Ca/P) increases the acidity and calcium phosphate solubility. For stoichiometric HA, the molar ratio of Ca/P is 1.67 [9]. Due to the high chemical stability and the active chemical bonding with the natural bone, HA is regarded as a biologically active substance [10]. However, the brittleness is the most critical limitation of HA (synthetic calcium phosphate) for implant applications. To surmount this problem, HA is generally mixed with polymeric and ceramic materials to form HA-ceramic or HA-polymer composites [1,11].

* Corresponding author. Tel.: +9874 3100 5214.
E-mail address: f.heidari@yu.ac.ir (F. Heidari).

https://doi.org/10.1016/j.ceramint.2019.12.157
Received 10 August 2019; Received in revised form 14 December 2019; Accepted 17 December 2019
Available online 24 December 2019

Barium titanate (BT), with a perovskite structure, is a common ceramic material with high dielectric, ferroelectric, mechanical, thermal, and biocompatibility properties [8]. In many *in vivo* and *in vitro* studies, BT piezoceramic showed significant bioactivity due to the polarization process and appropriate biological responses [12]. According to Genchi et al. [13], BT nanoparticles with high biocompatibility are outstanding candidates for medical and therapeutic uses, such as delivery capsules, imaging probes, tissue engineering, and nanotechnology. Today, a lot of efforts have been made to change the structure and composition of biocomposites and improve the mechanical, physical, and biocompatible properties through the modification of construction methods. HA-BT composite is one of the most outstanding ceramic-ceramic biocomposites, which is suitable for electroactive orthopedic applications [8]. Baxter et al. [14], believe that polar HA/BT composite, due to the proliferation and differentiation of bone cells—and ultimately the appropriate biological responses *in vitro* experiments—has a high potential in clinical applications. The bioactivity of HA-BT composite is also proven by Tang et al. [15]. They showed that the osteoblasts of the culture medium, after three days, were propagated on the surface of the BT-HA composite produced by spark plasma sintering (SPS). Jianqing et al. [16], provided that the formation of new bone tissue at the loading surface of HA-BT biocomposite has brought about better bioactivity than that of pure HA. Also, according to the *in vivo* studies, it is possible to absorb calcium ions (Ca^{+2}) on the surface of the HA-BT composite by the polarization process, which is because of the biocompatibility of this composite in *in vivo* experiments [17]. Since the electrical properties of the natural bone play an important role in the recovery and bone resorption [18,19], the presence of BT with high biocompatibility and dielectric properties can provide the electrical properties of healthy bone [13,20]. In another study Dubay et al. [21], declared that the presence of BT particles in a SPS-ed HA-BT composite increased the mechanical (hardness and fracture toughness) and physical properties of the composite. Wang et al. [22], showed that the addition of BT to the HA matrix as a secondary phase, increased the fracture toughness of the matrix. In fact, the presence of BT particles has a direct effect on the crack propagation in this composite. Bowen et al. [23], studied the relationship between the composition and piezoelectric and dielectric properties of HA-BT composite. According to their results, the electrical properties of HA-BT composite depend on the volume fraction and dimensional ratio of BT particles, and the shape and the amount of porosities in the HA matrix [23]. In fact, the piezoelectric coefficient decreases with lowering the matrix stiffness (by adding porosity) and the alignment of BT particles in the polarization direction. Additionally, Bowen et al. [24], showed that in SPS-ed HA-BT composite, the presence of BT with high electrical properties improved the electrical properties of pure HA. Tang and Dubey et al. [12,15], have investigated the effect of composition on the mechanical properties of the HA-BT composites. They showed that increasing the BT content with high bonding energy, results in better mechanical properties of these composites.

Although over the last few years a considerable number of publications have been reported, no detailed study has been performed on the fabrication of HA-BT scaffolds by isostatic pressing. Besides, only a few studies have reported the mechanical and electrical properties of the HA-BT nanocomposite scaffold in a nonpolar state. Given this, in this study, HA was synthesized from sol-gel method and HA-BT nanocomposite scaffolds have been fabricated by pressure-less sintering method. The effects of BT nanoparticles on dielectric, piezoelectric and mechanical properties (hardness, compressive strength, and fracture toughness) are investigated. As, there are a few evidences on biocompatibility (Cell culture) and bioactivity of HA-BT nanocomposite scaffolds, the evaluation of the bioactivity of the composites with *in vitro* experiments and investigating the possibility of using HA-bioactive ceramic composite as an alternative to bone grafting are other objectives of the present study.

2. Materials and methods

2.1. Synthesis of hydroxyapatite powder by sol-gel method

The raw materials of calcium nitrate ($Ca(NO_3)_2.4H_2O$, Merck) and ammonium dihydrogen phosphate (H_6NO_4P, Merck) were weighted according to the stoichiometric formula and individually diluted with 500 ml of distilled water. To reach a pH = 11, we added the ammonia (NH_3) solution to each of the above solutions. Finally, the ammonia and calcium nitrate solution was added to ammonia and ammonium dihydrogen phosphate solution, and the mixture was stirred for 24 h (h) on a hot plate, so that the precipitation could occur. In the next step, the gel was washed with distilled water using a filter paper to reach a pH = 7 and finally dried at 100 °C for 24 h. The calcination process was carried out at 700 °C for 1 h with a heating and cooling rate of 5 °C/min to produce HA nanopowder [25].

2.2. Preparation of composite powder of HA-BT (0 to 100 wt% of BT)

Stoichiometric amounts of synthesized HA powder and commercially BT containing 0, 40%, 50%, 60% and 100 %wt BT (HA-x BT, x represents the weight percentage of BT) were mixed in a planetary mill using a polymeric jar and zirconia balls at 180 rpm for 2 h. After drying, the powders were uniaxially pressed into disks with a diameter of 10 mm and a thickness of ~1.5 mm. Further compaction was achieved by cold isostatic pressing (K CIP 303, Iran) at 250 MPa. Finally, all samples were sintered at a temperature of 1300 °C for 2 h.

2.3. Materials characterization

2.3.1. Morphology and composition

To investigate the morphology and study the microstructure of the cross-sectional areas of composite and pure samples, transmission electron microscopy (TEM), and scanning electron microscopy (SEM, TESCAN-Vega 3 model) were used. The phase composition was characterized by x-ray diffraction (XRD; D8 Advance, Bruker Inc., Germany) using Cu Kα radiation. Energy dispersive x-ray spectroscopy (EDS) and Fourier transform infrared spectroscopy (FTIR, Shimadzu 8300 model) were used to study the chemical composition and the molecular structure, respectively.

2.3.2. Mechanical properties

To study the mechanical properties of composite and pure samples, both compressive strength and hardness values were measured. The compressive strength test was performed on cylindrical specimens with a diameter of 10 mm and a thickness of 10 mm by using a Zwick/Roell Universal testing machine with a speed of 0.5 mm/min and 10 kN load cell. Disk-shaped samples with a diameter of 8 mm and a thickness of 3 mm were selected for the Vickers hardness test (MHV1000Z), and the test was performed with a load of 200 g and a dwell time of 10 s.

2.3.3. Electrical properties

For electrical measurements, disk shape samples were coated with silver paste and annealed at 800 °C. Room temperature capacitance and dielectric loss of all samples were measured by LCR meter (LCR-6020 GwInSTEK) at 1 kHz. For piezoelectric measurements, poling was carried out by applying a DC electric field of 4 kV/mm to the samples at room temperature for 20 min piezoelectric coefficients of pure HA, pure BT, and HA-BT composites were measured by using a d_{33} meter device (model YE2730).

2.3.4. In vitro biodegradability

To evaluate the bioactivity of pure BT, pure HA and HA-BT samples, a simulated body fluid (SBF) were prepared according to the proposed instruction of Kukobo [26], and all samples were immersed in SBF solution with a temperature of 37 °C for 28 days. After that, SEM and

atomic force microscopy (AFM) were used to observe the morphology and topography of pure and composite samples.

2.3.5. Biocompatibility

Cell studies were carried out using dental pulp stem cells (DPSCs). DPSCs were isolated from extracted teeth, which were collected from the Department of Oral Surgery at Marquette University, with informed consent and approval of Marquette University graduate school. Isolation of DPSCs was conducted as reported previously. Briefly, pulp tissues were cut into small pieces and were enzymatically digested by 0.4% w/v Dispase II and 0.3% w/v Collagenase for 30 min. After centrifugation, the pellet was suspended in culture medium containing Dulbecco's Minimum Essential Medium (DMEM; Invitrogen, NY, USA), 10% fetal bovine serum (FBS; Sigma, USA), 1% antibiotic-antimycotic (Invitrogen) and incubated at 37 °C and 5% CO_2. After reaching 80% confluency, cells were passaged with 0.25% trypsin/EDTA (Gibco). DPSCs at passage three to four were used for biocompatibility assays.

The sterilization of composite discs was accomplished using 70% ethanol for 20 min. After rinsing discs with phosphate-buffered saline (PBS; Sigma Aldrich, UK) and soaking in complete culture medium overnight, DPSCs were seeded on their surface. After counting the cells with a hemocytometer, suspension of 20,000 cells/sample were seeded on the surface of discs. After 2 h incubation at 37 °C with 5% CO_2, 500 µl of culture medium was added to each well. In 1, 3, and 7 days after cell seeding, the proliferation of DPSCS grown on the cell-loaded samples was evaluated by ProstoBlue assay. Samples were rinsed with PBS before adding ProstoBlue solution (Invitrogen, NY, USA). ProstoBlue solution in a ratio of 1:10 was prepared in phenol red-free DMEM and added to each well. Following 1 h incubation at 37 °C, 100 µL of colored media was transferred into a 96-well plate, and the fluorescence intensity at excitation wavelengths of 540 and emission wavelengths of 590 was measured by a microplate reader (Synergy HTX, BioTEK).

The viability of DPSCs on the composite scaffolds was also evaluated qualitatively using live/dead staining (LIVE/DEAD, Life Technologies, California, USA). One set of samples after one day of cell seeding were transferred into a new plate and rinsed with PBS. Loaded-cell samples were incubated in a mixture of 5 µM calcein-AM and 4 µM ethidium homodimer-1 in PBS for 15 min. Conversion of calcein AM to fluorescent calcein in live cells and penetration of Ethidium homodimer into cell membranes of dead cells allow the staining of cells. After washing again with PBS, live and dead cells were evaluated under an Olympus microscope (Evos Fluorescent, life technologies).

Alkaline phosphatase assay kit (Abcam, Cambridge, MA, USA) was also used for measuring ALP activity of cells seeded on samples. At 3 and 7 days after cell seeding, the samples were rinsed with PBS and lysed with assay buffer, as recommended by the manufacturer. After centrifugation at 13,000 g for 3 min, 50 µL 5 mM pNPP solution was added to 80 µL of each sample in 96-well plate, and the plate was incubated in the dark for 60 min at room temperature. Finally, the absorbance was read using a microplate reader (Synergy HTX, BioTEK) at 405 nm.

2.4. Statistical analysis

T-test and ANOVA were used to determine the relationship between the mean of data in each of the topics of mechanical, electrical, and biocompatibility properties.

3. Results and discussion

3.1. Characterization of synthesized and commercial powders

3.1.1. XRD analysis

Fig. 1a shows the XRD pattern of HA nanopowder produced by the sol-gel method at ambient temperature (25 °C). According to studies, the characteristic peaks in the following pattern are entirely in accordance with the standard XRD pattern (JCPDS, 00-024-0033), which is consistent with other researcher's reports [27,28]. Also, the characteristic peaks of HA phase at 2θ = 26° and 32° are observed in the XRD pattern. The peaks shown in Fig. 1a belong to the calcium oxide, β-tricalcium phosphate, and HA crystalline phases formed at 700 °C with an appropriate degree of crystallinity [29].

X-ray diffraction pattern of commercial BT powder is shown in Fig. 1b. As seen, in the pure perovskite BT with a tetragonal structure (JCPDS, 00-003-0725), no secondary phase was observed. The splitting of the peak at 2 θ = 45° confirms the ferroelectric nature of BT powder. XRD pattern of commercial BT is also consistent with the results of other studies [29].

Fig. 1c shows the XRD pattern of pure HA, pure BT, and 60 wt% BT-40 wt% HA composite samples sintered at 1300 °C. The intensity of the characteristic peak of BT phase at 2θ = 45° increases with increasing BT content (Fig. 1c). Additionally, the composite with 60 wt% BT had a broader peak than the other samples at 2θ = 45°. According to Vouilloz et al. [29], the reason for this behavior is the coexistence of cubic and tetragonal phases of BT. As shown in Fig. 1c, due to the increase in the weight percentage of the BT phase in 60 wt% BT-40 wt% HA composite, the intensity of the characteristic HA peaks at the 2θ angles of 26° and 32° also decreases. The XRD analysis for the composite containing 60 wt % BT confirms the presence of $CaTiO_3$ and barium phosphate ($Ba_3(PO_4)$) secondary phases. Therefore, in HA-BT composites the formation of secondary phases is possible, and the coexistence of the BT and HA phases during the sintering process [29] is also reported by Baxter and Vouilloz et al. [14,29].

3.1.2. FTIR analysis

Fig. 1d shows the FTIR pattern of HA nanopowder produced by the sol-gel method. In this pattern, the wavenumber 3419.17 cm-1 refers to the stretching band, while 630 cm-1 and 3560 cm-1 wavenumbers relate to the liberation band of OH- group. Additionally, the bands at 470.54, 570.83, 601.7, 960, 1050 and 1090 cm-1 originate from PO43- ions. According to this pattern, a free CO2 peak is observed at 2365 cm-1. The wavenumbers of 1415.7, 870 and 1450 cm-1 correspond to the characteristic peaks of the CO32- ions, respectively. The FTIR spectrum of sol-gel synthesized HA nanopowder are quite similar to the results of synthetic and natural HA nanoparticles [8].

3.1.3. TEM analysis

The TEM micrograph of HA-BT powder is shown in Fig. 2a. Accordingly, the spherical nanoparticles of BT and HA are clearly seen. Additionally, the HA-BT composite powder contains BT and HA powders with 50 and 200 nm, respectively. A uniform distribution of very fine BT and HA particles is also shown in Fig. 2a.

3.3. SEM analysis

The SEM micrographs of pure HA, pure BT, 60 wt% BT-40 wt% HA, 50 wt% BT-50 wt% HA and 40 wt% BT-60 wt% HA samples sintered at 1300 °C for 2 h are shown in Fig. 2(b-f). According to Fig. 2b, the microstructure of pure BT is dense, and porosities are uniformly distributed between the grains. The cross-sectional micrographs of pure HA are shown in Fig. 2c. A porous microstructure with small agglomerates is observed in this Figure (grains $^{<}$2 µm). As seen in Fig. 2d, the composite containing 60 wt% BT has lower porosities and a denser microstructure. As demonstrated in Fig. 2e, the composite containing 50 wt% BT has a somewhat dense microstructure with micrometer porosities ranging from 0.2 µm to 1.5 µm. The presence of more porosities in this composite compared to the 60 wt% BT-40 wt% HA composites can be attributed to the coexistence of BT and HA phases and the formation of secondary phases of calcium titanate and barium phosphate [29]. As observed in Fig. 2f, small and large porosities are distributed between the grains of the sample containing 40 wt% BT. It

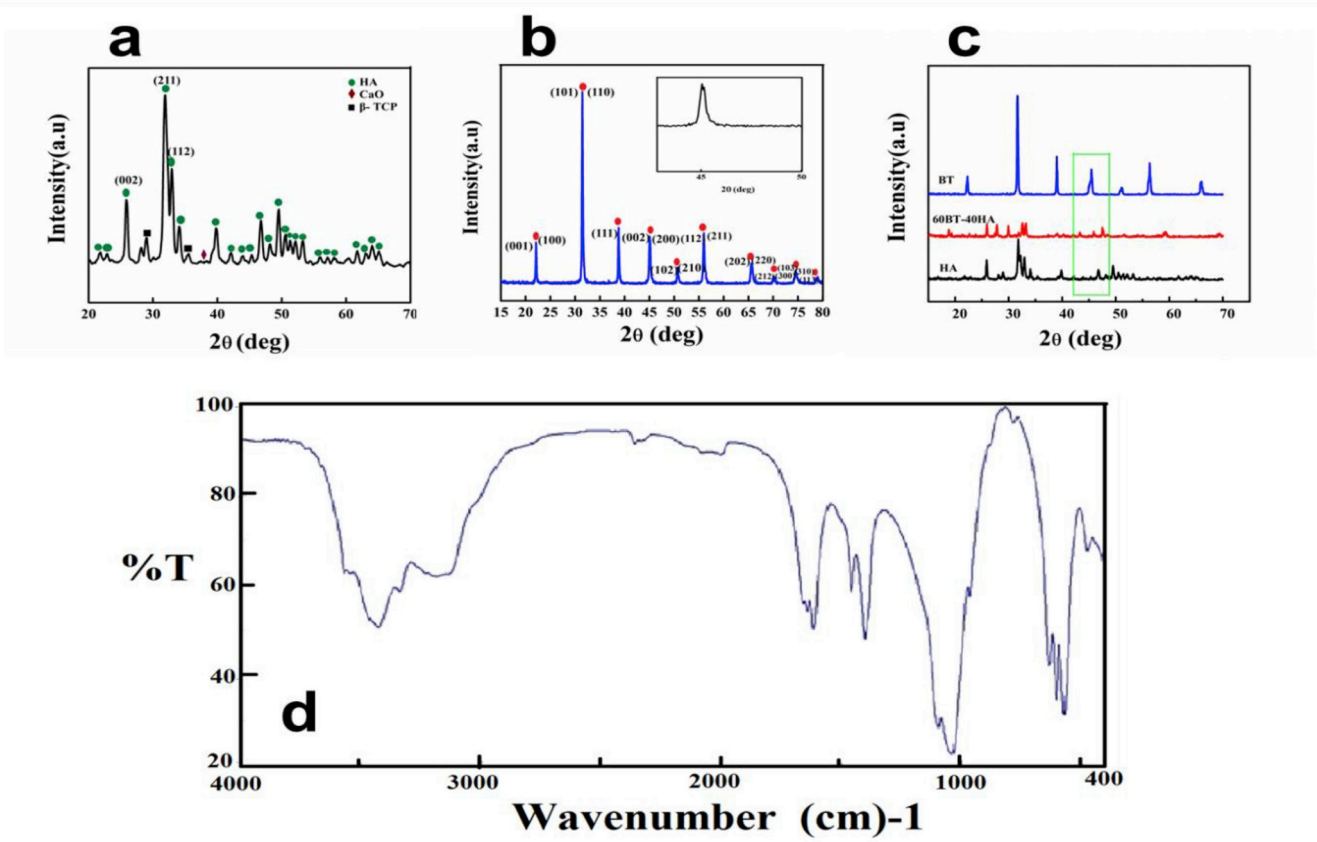

Fig. 1. X-ray diffraction pattern of a) synthesized HA, b) commercial BT and c) 60 wt% BT-40 wt% HA composite samples sintered at 1300 °C; d) FTIR pattern of sol-gel synthesized HA powder.

should be noted that at 1300 °C, the HA phase is more prone to decompose, and the liquid phase formation is possible [29]. Therefore, by decomposition of the HA phase, beta-tertiary calcium phosphate phases and the intermediate phase of HA can be formed with a gradual reduction of H_2O in the HA matrix [30], creating porosities in the samples.

Therefore, by comparing the SM images of the 60 wt% BT-40 wt% HA, 50 wt% BT-50 wt% HA and 40 wt% BT-60 wt% HA composite samples, it can be expected that with the addition of BT, the amount of porosity in the microstructure and the possibility of secondary phase formation will be reduced.

3.4. Mechanical properties

As it is shown in Fig. 3a, the highest bulk density is related to the composite of 60 wt% BT-40 wt% HA. Since the density of pure BT (6.02 g/cm^3) is higher than pure HA (2.83 g/cm^3), by increasing the content of BT in the HA-BT composite, the bulk density increases with

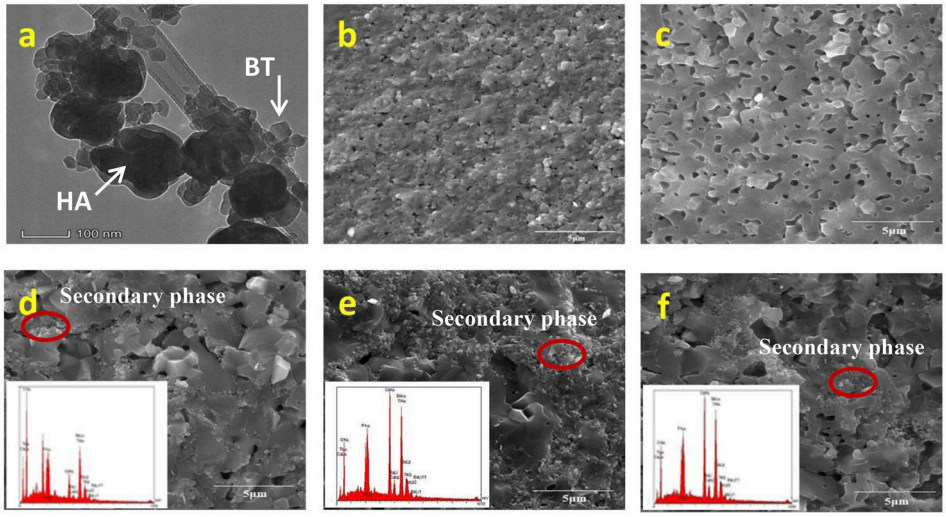

Fig. 2. a) TEM micrograph of the HA- BT composite powder and SEM microstructures of HA-BT samples sintered at 1300 °C: b) pure BT, c) pure HA, d) 60 wt% BT-40 wt% HA, e) 50 wt% BT-50 wt% HA, f) 40 wt% BT-60 wt% HA and EDS analysis of secondary phases.

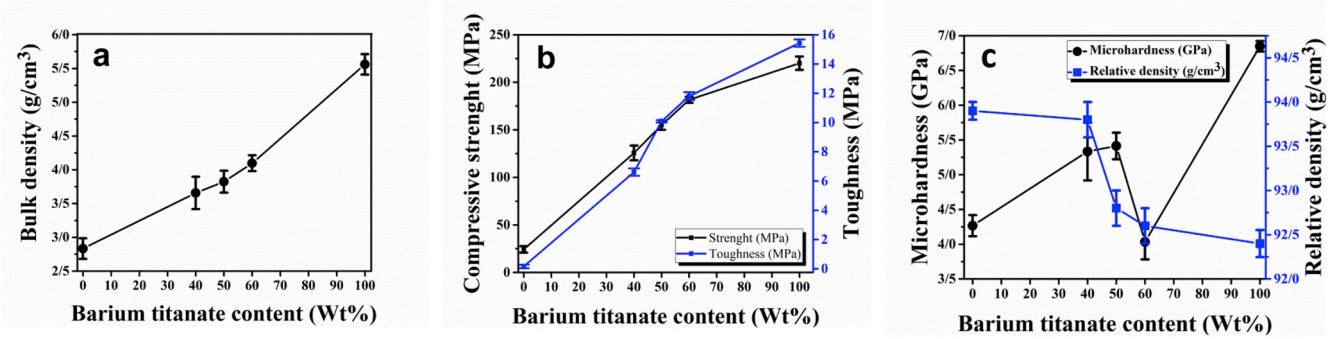

Fig. 3. The effect of BT content on a) bulk density, b) compressive strength and toughness, and c) microhardness and relative density of the HA- BT composites.

BT content, and the density of composite samples should be compared with the theoretical density of that composition. This phenomenon can be attributed to the decrease in the amount of HA, porosity and secondary phase present in the microstructure. The lowest value of bulk density belongs to 40 wt% BT-60 wt% HA composite. This can be attributed to the presence of secondary phases of barium phosphate, hydrogen phosphate, barium calcium, beta-tricalcium phosphate, and barium titanate phosphate [29]. Porosities, decomposition of HA, and the coexistence of HA and BT phase in HA-BT composite with 50 wt% BT are expected to be lower than the composite containing 40 wt% BT. As a result, by increasing the amount of HA, the formation of secondary phases is accelerated and, subsequently, larger amounts of porosities are created [29]. The calculated bulk density value for pure HA is higher than the corresponding value measured by Vouilloz et al. [32], for similar pressureless sintered samples. The Archimedes bulk density of pure BT was approximately similar to the value reported in this study [29]. In another study by Alock et al. [31], the optimum bulk density of sol-gel synthesized HA- 40 wt% BT (3.1 g/cm3) was less than this study.

According to Sikder *et al.* [32], the bulk density of conventionally sintered 40 wt% BT-60 wt% HA composite is 2.55 g/cm^3, which is also inferior than the bulk density value for a 40 wt% BT-60 wt% HA composite of this study. The difference in the calculated bulk density can be attributed to differences in the manufacturing method, sintering temperature and microstructure of the composite.

The diagram of compressive strength for pure BT, pure HA, and BT-HA composite samples after sintering at 1300 °C for 2 h is shown in Fig. 3b. The compressive strengths values for pure HA, and BT are 24.2 MPa and 220 MPa, respectively. According to Fig. 3b, by adding BT to HA, the compressive strength of composite samples increases compared to pure HA ($p > 0.05$). This can be attributed to the presence of BT with higher density, which reduces the porosities due to secondary phases and the decomposition of HA in HA-BT composite, which helps to increase the compressive strength of samples.

The initial particle size of HA and BT also affects compressive strength values of dense samples. The addition of the nano-particle secondary phase to the ceramic matrix increases the surface-to-volume ratio, and the compressive force is applied to a larger cross-sectional area. Finally, with higher compressive forces, the fracture occurs [33]. The amounts of vertical and parallel compressive strengths for the normal bone are 133 MPa and 170–193 MPa [34], however, 60 wt% BT-40 wt% HA composite can tolerate greater compressive strength than normal human bone. As a result, a composite of 60 wt% BT-40 wt % HA can be considered as an optimal composite with considerable compressive strength. The results of compressive strength for all samples are higher than the results obtained by Tang et al. [15], for both pure and composite (90 wt% BT -10 wt% HA and 80 wt% BT -20 wt% HA) samples produced by casting.

In two separate studies, Dubey et al. [10,21], reported the compressive strengths of 138.3 and 236 Mpa for SP-ed composites containing 40 wt% BT, which were higher than the compressive strength of normal bone (131 Mpa). Accordingly, the amounts of compressive strengths of 50 wt% BT-50 wt% HA and 60 wt% BT-40 wt% HA composites of this study are greater than the compressive strength of normal bone.

In general, the nature of the primary powder, grain size, and sintering temperature are the essential factors in determining the toughness [35]. As shown in Fig. 3b, pure BT has higher toughness than pure HA, so the presence of BT secondary phase with higher toughness increases the toughness of the HA-BT composite in comparison with pure HA ($p > 0.05$). So far, the toughness of isostatic-pressed HA-BT composite samples is not reported elsewhere.

Hardness refers to the resistance of a material against the plastic deformation or the strength of a material against the indentation at the surface. According to the previous studies, pure BT sample has the highest degree of Vickers hardness compared with other samples, which can be attributed to the high bonding energy between oxygen and barium ions (561.9 ± 13.4 KJ/mol) ($p > 0.05$) [36]. Therefore, with increased bonding energy, further activation energy is required for bond failure and probably in the presence of BT, even with a low weight percentage, the composite hardness increases. On the other hand, according to the hall patches equation, with decreasing the grain size, the yield stress also increases [37]. As a result, during the hardness test, plastic deformation occurs at higher stresses. Therefore, it can be said that the presence of BT with small grains in the HA matrix can increase the hardness ($p > 0.05$) (Fig. 3c). According to Zysset et al. [38], the hardness of natural human bone is in the range of 0.23 to 0.76 GPa. Considering this value, the presence of BT with different weight percentages (40, 50 and 60 wt%) in the matrix of HA increases the hardness to values higher than that of normal bone. On the other hand, as shown in Fig. 3c, increasing the relative density leads to a reduction in hardness. Hardness values of pure HA and 40 wt% BT-60 wt% HA composite are higher than the corresponding results of Sikder *et al.* [32], for conventionally sintered samples. However, they are lower than the hardness values of SP-ed pure HA, 40 wt% BT-60 wt% HA and 60 wt% BT-40 wt% HA samples reported by Dubey et al. [21]. Although, the hardness decreased, the presence of BT improved the hardness of the matrix phase, so that the hardness measured for the samples mentioned was greater than normal bone. On the other hand, the method mentioned in this study for the prepared of HA-BT composite is economical compared to the SPS method. In fact, the difference in the reported hardness values can be attributed to differences in the method of manufacture, sinter and microstructure of the HA-BT composite. It is important to note that the presence of 50 wt% BT improved the hardness of the matrix HA phase. By comparing the hardness values obtained for the 40 wt% BT-60 wt% HA, 50 wt% BT-50 wt% HA and 40 wt% BT-60 wt% HA composites, it can be said that the composite containing 50 wt% BT has the highest hardness than other composites. According to the study by Dubey et al. [10], only the compressive strength of the 40 wt% BT-60 wt% HA, 50 wt% BT-50 wt% HA composites have been investigated and the hardness has not been measured for the mentioned composites. It should be noted that there is not much research on the microstructure, physical and mechanical properties of

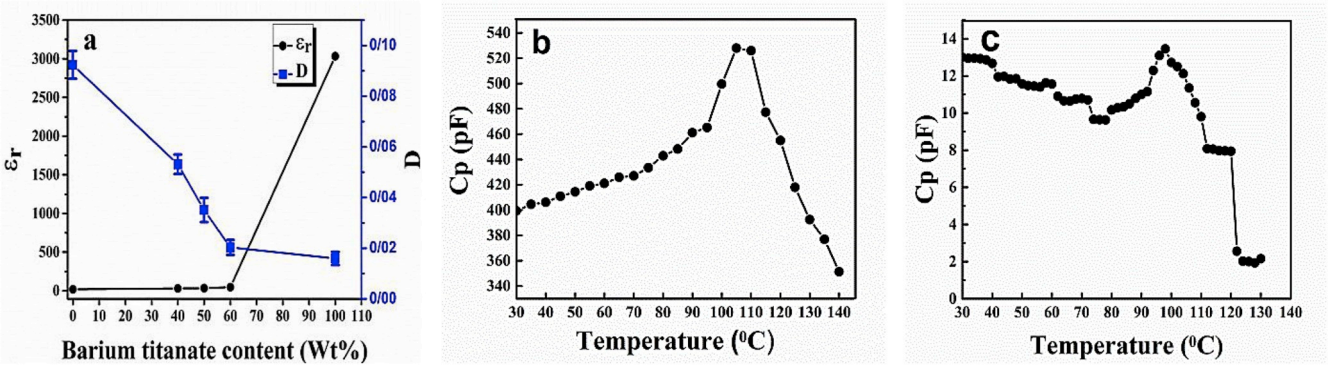

Fig. 4. a) The variations in dielectric constant and loss for pure and composite samples at the frequency of 1 kHz and Curie temperature of b) pure BT and c) 60 wt% BT-40 wt% HA composite at 1 kHz frequency.

composite containing 50 wt% BT and the information provided in this study is for reporting.

An important and similar point in this study to other studies is that the addition of BT with different weight percentages improves the mechanical properties of the HA phase.

3.5. Dielectric and electrical behavior

According to Fig. 4a, by increasing the BT content, the dielectric loss (D) of the composite samples decreases. The reason is the lower amount of porosities and the higher densities of composite samples compared with pure HA [29]. The composite sample containing 60 wt% BT shows the smallest amount of dielectric loss at the frequency of 1 kHz ($p > 0.05$). According to Pen et al. [39], studies, a high value of tan δ is attributed to the trapping of electrons inside the cavities.

In this study, the dielectric loss values of pure BT, pure HA, and 40 wt% BT-60 wt% HA composite samples are lower than those reported by Bowen et al. [24] (samples made by pressureless sintering). For 60 wt% BT-40 wt% HA composite sample, the measured tan δ is lower than the results of Dubey et al. [12], for similar composite (made by SPS). The variations in the dielectric constant (ε_r) of all composites with BT content are shown in Fig. 4a. The 60 wt% BT-40 wt% HA composite with a dielectric constant of 46.50 has the highest value compared to other composite samples. Therefore, the coupling of low-dielectric constant HA with BT causes a sudden decrease in the capacity and dielectric constant of all composite samples compared with pure BT ($p < 0.05$). In fact, due to the development of parallel polarization in the presence of two phases with different weight percentages and different electrical conductivity, a composite sample containing 60 wt% BT has the highest amount of dielectric constant and lower dielectric loss at room temperature, along with a low frequency of 1 kHz compared to other composites ($p > 0.05$). Based on previous studies, factors influencing the dielectric constant are microstructure, distribution of crystalline phases alongside each other, and the density of the sample [24,29]. The dielectric constants values of 60 wt% BT-40 wt% HA and 40 wt% BT-60 wt% HA composite samples of this study are higher than the results reported by Dubey et al. [12], for similar composites made by SPS. According to the reports of Bowen et al. [24], The dielectric constant of pressureless sintered BT sintered by pressureless sintering method is less than the dielectric constant of the pure BT sample of this study. Additionally, the measured dielectric constant value for pure HA sample is lower than the results reported by Bowen et al. [24].

The values of dielectric loss and dielectric constant of HA-BTcomposite containing 50 wt% BT are than than 60 wt% BT-40 wt% HA and higher than 40 wt% BT-60 wt% HA composites. This difference can be attributed to the weight percent of BT, the amount of porosities in the microstructure, the presence of secondary phases, and the sample density.

The piezoelectric coefficient of pure BT is approximately 28 pC/N. Since the piezoelectric coefficient decreases with decreasing the grain size [40], the piezoelectric coefficient measured for pure BT is also lower than the reported value of Vouilloz et al. [29]. It can be attributed to the lesser degree of freedom of the spheres during the polarization process and the inhibition of adjacent grains to form a bipolar domain in other grains [41]. Although, the piezoelectric coefficient of BT is higher than the corresponding values reported for normal bone (0.7 PC/N) [29], the piezoelectric coefficient of pure HA is almost zero, which is in agreement with the values reported by Dubey et al. [21]. The piezoelectric coefficients of all composite samples are approximately zero. According to Bowen et al. [24], piezoelectric coefficients greater than zero can be expected for composites containing more than 80 wt% BT.

Fig. 4 b and c demonstrate the temperature dependence of the dielectric constant for pure BT and the 60 wt% BT-40 wt% HA composite samples. As seen, the Curie temperature for pure BT and the 60 wt% BT-40 wt% HA composite samples are 110 °C and 97 °C, respectively. However, the Curie temperature of micron-sized BT reported in the literature is about 120 °C [40]. For 60 wt% BT- 40 wt% HA composite sample with nano-sized grains, this value ranges from 97 °C to 122 °C [42]. According to Tan et al. [40], decreasing the grain size reduces the Curie temperature.

3.6. Bioactivity evaluation

Fig. 5 (a, c and d) shows the SEM images of pure HA, composite 60 wt% BT-40 wt% HA and pure BT samples immersed in SBF solution for 28 days. It should be noted that only the bioactivity of the 60 wt% BT-40 wt% HA composite has been studied among other composites. The reason for this choice is the optimum microstructure and mechanical properties of this composite compared to other composites. Fig. 5a shows the morphology of the apatite crystals formed on the pure HA sample.

According to Fig. 5a, the surface of the sample is completely covered with a layer of apatite crystals. The EDS pattern of the apatite formed on the surface of the pure HA sample after immersion in the SBF is shown in the left corner of Fig. 5a. In this pattern (Fig. 5a), the characteristic peak of the apatite-containing elements—including Ca, P, and O—have high intensity. In fact, by immersing in the SBF, the ions in the SBF solution move towards the sample surface. In this case, the entry of ions—and even their dissolution at the sample surface—provide nucleation areas with less surface energy for nucleation of apatite crystals [43].

On the other hand, according to Kokubo et al. [26], the apatite crystals formed on the surface of ceramic and composite samples have a Ca/P ratio of 1.67. The morphology of 60 wt% BT-40 w% HA composite and pure BT samples are shown in Fig. 5 c and d, respectively, it can be seen that apatite crystals and NaCl salt formed on the surface of the

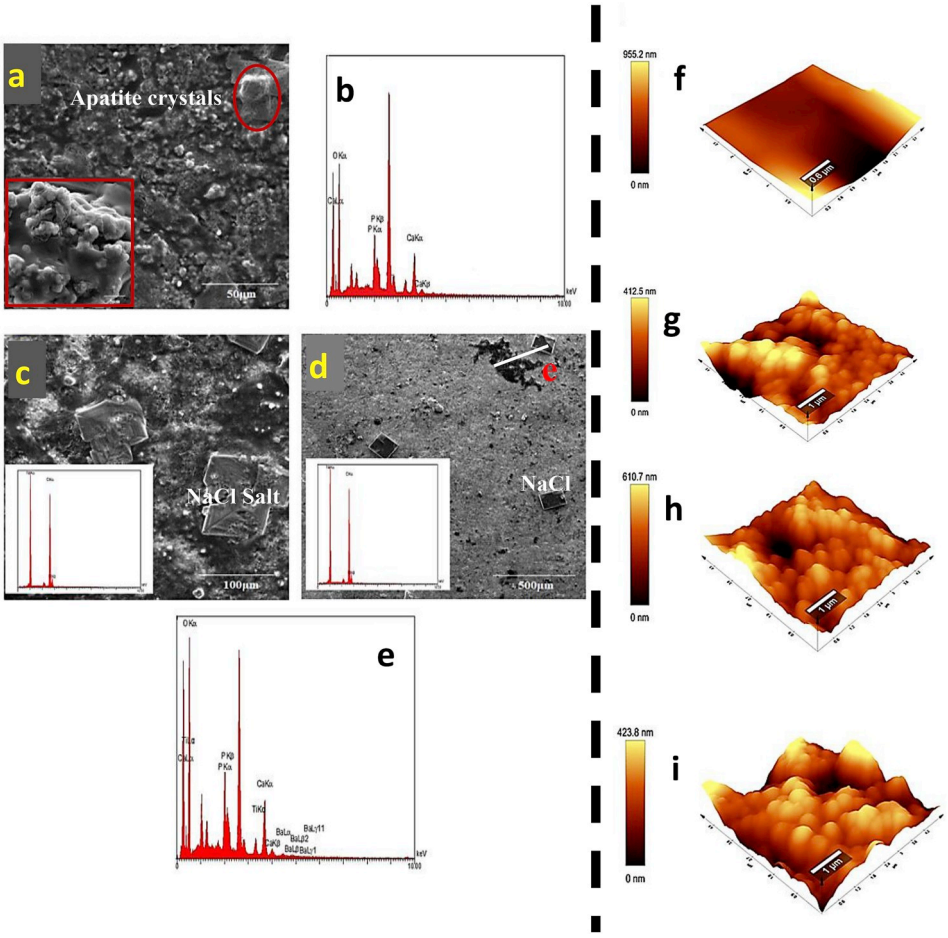

Fig. 5. Morphology of apatite crystals formed on the surface of samples after immersion in SBF: a) pure HA, b) line EDS analysis of apatite crystal formed on the surface of pure HA, c) 60 wt% BT- 40 wt% HA composite, d) pure BT, e) line EDS analysis from HA and BT phases and salt deposits of NaCl. AFM topography of (f, g) pure HA and (h, i) 60 wt% BT-40 wt% HA composite, before and after immersion in the SBF, respectively.

samples. In fact, the formation of NaCl salt deposits on the surface of both samples due to the insolubility, and no entry of ions into the sample surface at locations with the presence of BT phase. In this case, the places of apatite nucleation reduced. However, in the 60 wt% BT-40 wt% HA composite sample due to the presence of HA, the number of apatite crystals formed on the surface increased compared with pure BT sample. Because fine particles of HA in the composite, help to absorb and deposit minerals with calcium content [36]. As a result, according to the pattern of EDS analysis shown in the left-hand side of Fig. 5c, the presence of salt crystals and the deviation from the Ca/P ratio of 1.67 for apatite crystals formed on the surface of 60 wt% BT-40 wt% HA composite, this composite does not have a biomedical application [26]. Finally, the EDS pattern in Fig. 5e confirms the presence of Ca, P, O, Ba, Ti, Na, and Cl elements on the surface of pure BT.

To demonstrate the formation of apatite crystals on the surface of pure HA and 60 wt% BT-40 wt% HA composite, we examined the surface topography of the samples before and after immersion in SBF. By comparing the images in Fig. 5 f and g and reducing the roughness of 542.7 for a pure HA sample, it can be concluded that the sedimentation of apatite after immersion in SBF is completely uniform on the surface of the pure HA sample. According to studies of Kokubo et al. [26], the formation of a surface layer of apatite crystals on the surface of ceramic and composite samples after immersion in SBF indicates the bioactivity of the samples. Consequently, the presence of apatite crystals on the surface of the HA sample by atomic force microscopy indicates the bioactivity of the pure HA sample. According to Fig. 5 h and i, the roughness reduction of the 60 wt% BT-40 wt% HA composite sample due to apatite and salt depositions on the surface, was 186.9 nm.

On the other hand, by comparing Fig. 5 g and i, the apatite sediments formed on the surface of the pure HA sample were much more uniform than 60 wt% BT-40 wt% HA composite. The weight changes of the samples (Table 1) before and after immersion in SBF confirm the presence of the apatite crystals on the surface of the samples. Also, by decreasing the HA content in the 60 wt% BT-40 wt% HA composite, a considerable weight change after immersion in SBF solution have been observed. This behavior indicates the contribution of BT in preferential apatite precipitation around the HA grains in this sample.

In this paper, the bioactivity of samples is evaluated in the absence

Table 1
Weight changes of pure HA and 60 wt% BT-40 wt% HA composite before and after immersion in SBF for 28 days.

Composition (Wt%)	Weight before immersion (g)	Weight after immersion (g)	Weight changes (g)
Pure HA	0.6827	0.6856	0.0029
60 wt% BT-40 wt% HA	0.2952	0.2979	0.0027
Pure BT	1.1901	1.1915	0.0014

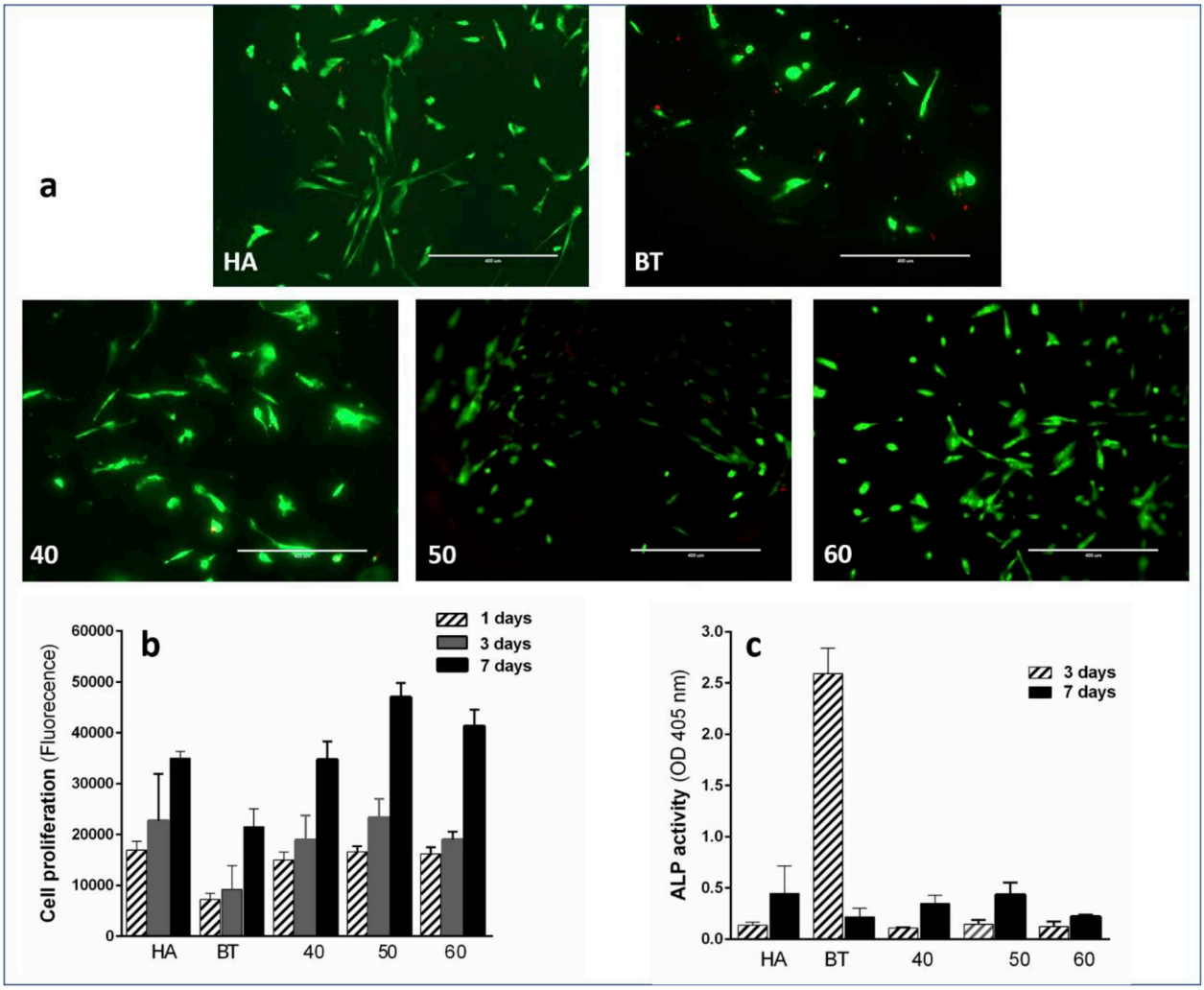

Fig. 6. a) Live/dead staining of DPSCs cultured for 1 day on pure HA, pure BT, and composite samples containing 40, 50 and 60 % wt BT. The live green cells seem to have normal morphology. Red dead cells were very few on all samples. b) Results of PrestoBlue assay after 1, 3, and 7 days culture of DPSCs on samples. c) Alkaline phosphatase activity (ALP). Each value is mean ± sd, n = 5. (For interpretation of the references to color in this figure legend, the reader is referred to the Web version of this article.)

of a polarization process. It was suggested that by polarizing the samples, more favorable conditions for the formation of apatite crystals on the surface of the specimens could be provided after immersion in the SBF solution. Mythili Prakasam et al. [42], obtained significant results for the formation of apatite crystals on immersed polar specimens, and we are also trying to investigate it in future studies.

3.7. Biocompatibility evaluation

The viability and proliferation of DPSCs on the scaffolds were determined both quantitatively by ProstoBlue assay and qualitatively, with live/dead staining. As shown in Fig. 6a, no evidence of cell death (red fluorescence) is observed on the surface of our scaffolds, and DPSC distribution and proliferation was similar in all composite scaffolds. Increasing the cell density with culture time in all samples confirm excellent biocompatibility and no cytotoxic effects of scaffold materials and process (Fig. 6b). Although there is no significant difference between composite scaffolds and pure HA in our study, Ohgaki et al. [44], reported reduced cell proliferation in the polarized composite samples compared to the pure HA. However, in the study of Dekhtyar et al. [45], an increase of cell proliferation was found on composite samples compared to pure HA surface. One explanation for the variations in cellular responses seen in these studies is that the scaffolds used in the various experiments have different surface roughness and topology; also, cell types used in the studies are different [19]. In this study, the cellular density on the pure BT scaffolds is significantly lower than that on the other scaffolds ($p < 0.05$). Therefore, although all samples could support the proliferation of cells over time, the pure BT scaffolds have less affinity for cell attachment and subsequent proliferation of seeded cells. There is no significant difference between the three composite scaffolds (40, 50, and 60% wt BT). Ciofani et al. [46], showed that even robust mechanical properties of the high percentage of BT doped poly(lactic-co-glycolic) acid/BT composite scaffolds are considerably higher than the low percentage structures, but cell proliferation is similar ($p > 0.05$). Also, Tang et al. [15], reported no significant difference in the growth of osteoblasts on the composite scaffolds containing different contents of BT (80 and 90 wt% BT) and found same biocompatibility as the pure HA in these composite samples.

As a final test, the ALP activity of DPSCs on pure and composite scaffolds was assessed (Fig. 6c). Interestingly, after a 3-day incubation, the ALP activity in pure BT is more than other groups ($p < 0.05$), but after 7 days there is no significant difference between all groups. This result is in contrast to the result of Tang et al. [15], who reported more ALP activity in pure HA than pure BT, 80 wt% BT-20 wt% HA and 90 wt % BT-10 wt% HA composites. However, the cell used in their study was

osteoblast. Teixeira et al. [47], reported similar ALP activity for cultures on the composite membrane containing BT and poly (vinylidene fluoride-trifluoroethylene) at 14 days. In this study, all samples were cultured in the regular culture medium. The effects of culturing samples in osteogenic medium and the impact of BT on the differentiation of stem cells should be considered in future research.

4. Conclusion

In this paper, composite samples of HA-BT were produced through mechanical milling and non-pressure sintering. Sol-gel synthesized HA and commercial BT were the two components of the composite. The production of composite samples of HA-BT has been used to improve the physical, mechanical, and electrical properties of these samples by using universal cold press and pressure-less sinter. In this way, the results obtained in this study are almost near the results reported in the spark plasma sintering method. The presence of BT as a secondary phase reduces the porosity and relative density and increases the bulk density and mechanical properties of composite samples, especially the 60 wt% BT-40 wt% HA composite. Improving the mechanical properties after adding up to 60 wt% BT can be attributed to the size of the initial particles of HA and BT, the number and size of the porosities in the composite and the activation energy needed to fracture the bonds. The results of biocompatibility assays show that all samples are biocompatible, and there is no significant difference between pure HA and composite scaffolds in term of cell proliferation and ALP activity.

Declaration of competing interest

The authors declare that they have no known competing financial interests or personal relationships that could have appeared to influence the work reported in this paper.

Acknowledgements

This work has formed part of research master plan of corresponding author (Fatemeh Heidari) and has been supported by Yasouj University. The authors gratefully acknowledge Deputy of Research and Technology of Yasouj University for financial support of the research project.

Appendix A. Supplementary data

Supplementary data to this article can be found online at https://doi.org/10.1016/j.ceramint.2019.12.157.

References

[1] B. Liu, L. Chen, C. Shao, F. Zhang, K. Zhou, J. Cao, D. Zhang, Improved osteoblasts growth on osteomimetic hydroxyapatite/BaTiO3 composites with aligned lamellar porous structure, Mater. Sci. Eng. C 61 (2016) 8–14, https://doi.org/10.1016/j.msec.2015.12.009.
[2] R. Cancedda, P. Giannoni, M. Mastrogiacomo, A tissue engineering approach to bone repair in large animal models and in clinical practice, Biomaterials 28 (2007) 4240–4250, https://doi.org/10.1016/j.biomaterials.2007.06.023.
[3] E. Fukada, I. Yasuda, On the piezoelectric effect of bone, J. Phys. Soc. Jpn. 12 (1957) 1158–1162, https://doi.org/10.1143/JPSJ.12.1158.
[4] A. Dubey, K. Balani, B. Basu, Electrically active biocomposites as smart scaffolds for bone tissue engineering, Nanomedicine (2012) 537–570, https://doi.org/10.1533/9780857096449.4.537.
[5] C.A.L. Bassett, R.O. Becker, Generation of electric potentials by bone in response to mechanical stress, Science 137 (1962) 1063–1064, https://doi.org/10.1126/science.137.3535.1063.
[6] J. Park, R.S. Lakes, Biomaterials: an Introduction, Springer Science & Business Media, 2007.
[7] M. Kay, R. Young, A. Posner, Crystal structure of hydroxyapatite, ON Nat. 204 (1964) 1050, https://doi.org/10.1038/2041050a0.
[8] H. Zhou, J. Lee, Nanoscale hydroxyapatite particles for bone tissue engineering, Acta Biomater. 7 (2011) 2769–2781, https://doi.org/10.1016/j.actbio.2011.03.019.
[9] C. Chai, B. Ben-Nissan, Bioactive nanocrystalline sol-gel hydroxyapatite coatings, J. Mater. Sci. Mater. Med. 10 (1999) 465–469, https://doi.org/10.1023/A:1008992807888.
[10] A.K. Dubey, K.-i. Kakimoto, Impedance spectroscopy and mechanical response of porous nanophase hydroxyapatite–barium titanate composite, Mater. Sci. Eng. C 63 (2016) 211–221, https://doi.org/10.1016/j.msec.2016.02.027.
[11] A. Arifin, A.B. Sulong, N. Muhamad, J. Syarif, M.I. Ramli, Material processing of hydroxyapatite and titanium alloy (HA/Ti) composite as implant materials using powder metallurgy: a review, Mater. Des. 55 (2014) 165–175, https://doi.org/10.1016/j.matdes.2013.09.045.
[12] A. Dubey, B. Basu, K. Balani, R. Guo, A. Bhalla, Dielectric and pyroelectric properties of HAp-BaTiO3 composites, Ferroelectrics 423 (2011) 63–76, https://doi.org/10.1080/00150193.2011.618382.
[13] G.G. Genchi, A. Marino, A. Rocca, V. Mattoli, G. Ciofani, Barium titanate nanoparticles: promising multitasking vectors in nanomedicine, Nanotechnology 27 (2016), https://doi.org/10.1088/0957-4484/27/23/232001 232001.
[14] F.R. Baxter, I.G. Turner, C.R. Bowen, J.P. Gittings, J.B. Chaudhuri, An in vitro study of electrically active hydroxyapatite-barium titanate ceramics using Saos-2 cells, J. Mater. Sci. Mater. Med. 20 (2009) 1697–1708, https://doi.org/10.1007/s10856-009-3734-0.
[15] Y. Tang, C. Wu, Z. Wu, L. Hu, W. Zhang, K. Zhao, Fabrication and in vitro biological properties of piezoelectric bioceramics for bone regeneration, Sci. Rep. 7 (2017) 43360, https://doi.org/10.1038/srep43360.
[16] F. Jianqing, Y. Huipin, Z. Xingdong, Promotion of osteogenesis by a piezoelectric biological ceramic, Biomaterials 18 (1997) 1531–1534, https://doi.org/10.1016/S0142-9612(97)80004-X.
[17] A. Ravaglioli, A. Krajewski, Bioceramics and the Human Body, Springer Science & Business Media, 2012.
[18] N. Teng, S. Nakamura, Y. Takagi, Y. Yamashita, M. Ohgaki, K. Yamashita, A new approach to enhancement of bone formation by electrically polarized hydroxyapatite, J. Dent. Res. 80 (2001) 1925–1929, https://doi.org/10.1177/00220345010800101201.
[19] F.R. Baxter, C.R. Bowen, I.G. Turner, A.C. Dent, Electrically active bioceramics: a review of interfacial responses, Ann. Biomed. Eng. 38 (2010) 2079–2092, https://doi.org/10.1007/s10439-010-9977-6.
[20] A.K. Dubey, S.D. Gupta, B. Basu, Optimization of electrical stimulation parameters for enhanced cell proliferation on biomaterial surfaces, J. Biomed. Mater. Res. Part B. 98 (2011) 18–29, https://doi.org/10.1002/jbm.b.31827.
[21] A.K. Dubey, K. Balani, B. Basu, Multifunctional properties of multistage spark plasma sintered HA–BaTiO 3-based piezobiocomposites for bone replacement applications, J. Am. Ceram. Soc. 96 (2013) 3753–3759, https://doi.org/10.1111/jace.12566.
[22] H. Wang, R.N. Singh, Crack propagation in piezoelectric ceramics under pure mechanical loading, Ferroelectrics 207 (1998) 555–575, https://doi.org/10.1080/00150199808217269.
[23] C.R. Bowen, V.Y. Topolov, Piezoelectric activity and sensitivity of novel composites based on barium titanate-hydroxyapatite composite ceramics, Key Eng. Mater. (2007) 1113–1116 https://doi.org/10.4028/www.scientific.net/KEM.334-335.1113.
[24] C. Bowen, J. Gittings, I. Turner, F. Baxter, J. Chaudhuri, Dielectric and piezoelectric properties of hydroxyapatite-Ba Ti O 3 composites, Appl. Phys. Lett. 89 (2006), https://doi.org/10.1063/1.2355458 132906.
[25] M. Fathi, A. Hanifi, Evaluation and characterization of nanostructure hydroxyapatite powder prepared by simple sol–gel method, Mater. Lett. 61 (2007) 3978–3983, https://doi.org/10.1016/j.matlet.2007.01.08.
[26] T. Kokubo, H. Takadama, How useful is SBF in predicting in vivo bone bioactivity? Biomaterials 27 (2006) 2907–2915, https://doi.org/10.1016/j.biomaterials.2006.01.017.
[27] M. Bilton, A. Brown, S. Milne, Sol-gel synthesis and characterisation of nano-scale hydroxyapatite, J. Phys. Conf. Ser. (2010), https://doi.org/10.1088/1742-6596/241/1/012052 012052.
[28] B. Matthew, M. Steven J, B. Andrew P, Comparison of hydrothermal and sol-gel synthesis of nano-particulate hydroxyapatite by characterisation at the bulk and particle level, J. Inorg. Non-Metallic. Mater. 2012 (2012) 1–10, https://doi.org/10.4236/ojinm.2012.21001.
[29] F. Vouilloz, M.S. Castro, G.E. Vargas, A. Gorustovich, M.A. Fanovich, Reactivity of BaTiO3-Ca10 (PO4) 6 (OH) 2 phases in composite materials for biomedical applications, Ceram. Int. 43 (2017) 4212–4221, https://doi.org/10.1016/j.ceramint.2016.12.053.
[30] G. Muralithran, S. Ramesh, The effects of sintering temperature on the properties of hydroxyapatite, Ceram. Int. 26 (2000) 221–230, https://doi.org/10.1016/S0272-8842(99)00046-2.
[31] A.K. Panda, Preparation and Characterization of Hydroxyapatite-Barium Titanate Composite, (2011).
[32] P. Sikder, N. Koju, B. Lin, S.B. Bhaduri, Conventionally sintered hydroxyapatite–barium titanate piezo-biocomposites, Trans. Indian Inst. Met. 72 (2019) 2011–2018, https://doi.org/10.1007/s12666-018-1533-3.
[33] Y. Jung, S.S. Kim, Y.H. Kim, S.H. Kim, B.S. Kim, S. Kim, C.Y. Choi, S.H. Kim, A poly (lactic acid)/calcium metaphosphate composite for bone tissue engineering, Biomaterials 26 (2005) 6314–6322, https://doi.org/10.1016/j.biomaterials.2005.04.007.
[34] W. Suchanek, M. Yoshimura, Processing and properties of hydroxyapatite-based biomaterials for use as hard tissue replacement implants, J. Mater. Res. 13 (1998) 94–117, https://doi.org/10.1557/JMR.1998.0015.
[35] P. Kamalanathan, S. Ramesh, L. Bang, A. Niakan, C. Tan, J. Purbolaksono, H. Chandran, W. Teng, Synthesis and sintering of hydroxyapatite derived from eggshells as a calcium precursor, Ceram. Int. 40 (2014) 16349–16359, https://doi.

org/10.1016/j.ceramint.2014.07.074.
[36] T.J. Webster, C. Ergun, R.H. Doremus, R.W. Siegel, R. Bizios, Enhanced functions of osteoblasts on nanophase ceramics, Biomaterials 21 (2000) 1803–1810, https://doi.org/10.1016/S0142-9612(00)00075-2.
[37] C. Carlton, P.J. Ferreira, What is behind the inverse Hall–Petch effect in nanocrystalline materials? Acta Biomater. 55 (2007) 3749–3756, https://doi.org/10.1016/j.actamat.2007.02.021.
[38] P.K. Zysset, X.E. Guo, C.E. Hoffler, K.E. Moore, S.A. Goldstein, Elastic modulus and hardness of cortical and trabecular bone lamellae measured by nanoindentation in the human femur, J. Biomech. 32 (1999) 1005–1012, https://doi.org/10.1016/S0021-9290(99)00111-6.
[39] S.J. Penn, N.M. Alford, A. Templeton, X. Wang, M. Xu, M. Reece, K. Schrapel, Effect of porosity and grain size on the microwave dielectric properties of sintered alumina, J. Am. Ceram. Soc. 80 (1997) 1885–1888, https://doi.org/10.1111/j.1151-2916.1997.tb03066.x.
[40] Y. Tan, J. Zhang, Y. Wu, C. Wang, V. Koval, B. Shi, H. Ye, R. McKinnon, G. Viola, H. Yan, Unfolding grain size effects in barium titanate ferroelectric ceramics, Sci. Rep. 5 (2015) 9953, https://doi.org/10.1038/srep09953.
[41] W.S. Hackenberger, M.J. Pan, V. Vedula, P. Pertsch, W. Cao, C.A. Randall, T.R. Shrout, Effect of grain size on actuator properties of piezoelectric ceramics, Int. Soc. Opt. Photonics (1998) 28–36, https://doi.org/10.1117/12.316878.
[42] M. Prakasam, M. Albino, E. Lebraud, M. Maglione, C. Elissalde, A. Largeteau, Hydroxyapatite-barium titanate piezocomposites with enhanced electrical properties, J. Am. Ceram. Soc. 100 (2017) 2621–2631, https://doi.org/10.1111/jace.14801.
[43] F. Mohandes, M. Salavati-Niasari, Influence of morphology on the in vitro bioactivity of hydroxyapatite nanostructures prepared by precipitation method, New J. Chem. 38 (2014) 4501–4509, https://doi.org/10.1039/C4NJ00649F.
[44] M. Ohgaki, T. Kizuki, M. Katsura, K. Yamashita, Manipulation of selective cell adhesion and growth by surface charges of electrically polarized hydroxyapatite, J. Biomed. Mater. Res. 57 (2001) 366–373, https://doi.org/10.1016/j.msec.2015.12.009.
[45] Y. Dekhtyar, N. Polyaka, R. Sammons, 14th Nordic-Baltic Conference on Biomedical Engineering and Medical Physics, Springer, 2008.
[46] G. Ciofani, L. Ricotti, V. Mattoli, Preparation, characterization and in vitro testing of poly (lactic-co-glycolic) acid/barium titanate nanoparticle composites for enhanced cellular proliferation, Biomed. Microdevices 13 (2011) 255–266, https://doi.org/10.1007/s10544-010-9490-6.
[47] L. Teixeira, G. Crippa, A. Trabuco, R. Gimenes, M. Zaghete, D. Palioto, P. De Oliveira, A. Rosa, M. Beloti, In vitro biocompatibility of poly (vinylidene fluoride–trifluoroethylene)/barium titanate composite using cultures of human periodontal ligament fibroblasts and keratinocytes, Acta Biomater. 6 (2010) 979–989, https://doi.org/10.1016/j.actbio.2009.08.024.